PROPAGATION OF UHF RADIO WAVES IN LIMESTONE ROOM AND PILLAR MINES

Robert L. Lagace, Task Leader
Alfred G. Emslie

prepared for

UNITED STATES
DEPARTMENT OF THE INTERIOR
BUREAU OF MINES

by

ARTHUR D. LITTLE, INC.
CAMBRIDGE, MASSACHUSETTS

summary report

TASK ORDER NO. J0387217

UNDER BASIC AGREEMENT
J0377065

JANUARY 1979

Arthur D Little, Inc.

The views and conclusions contained in this document are those of the authors and should not be interpreted as necessarily representing the official policies or recommendations of the Interior Department's Bureau of Mines or of the U.S. Government.

REPORT DOCUMENTATION PAGE

1. Report No.	2.	3. Recipient's Accession No.

4. Title and Subtitle
PROPAGATION OF UHF RADIO WAVES IN LIMESTONE ROOM AND PILLAR MINES

5. Report Date
January 1979

6.

7. Author(s)
Robert L. Lagace, Task Leader
Alfred G. Emslie

8. Performing Organization Report No.
ADL-81863

9. Performing Organization Name and Address
Arthur D. Little, Inc.
25 Acorn Park
Cambridge, Massachusetts 02140

10. Project/Task/Work Unit No.

11. Contract or Grant No.
Task Order J0387217

12. Sponsoring Organization Name and Address
Office of the Assistant Director - Mining
Bureau of Mines
Department of the Interior
Washington, D. C. 20241

13. Type of Report
Summary
April 1978 - January 1979

14.

15. Supplementary Notes

16. Abstract

This report presents a mathematical model for the propagation of UHF radio waves in the large cross-section tunnels of a room and pillar limestone mine, and describes the analysis of a small amount of propagation data obtained in a limestone mine. The model and analysis is based on the waveguide mode theory developed earlier for the transmission of UHF waves in coal mine tunnels, with allowance for propagation losses due to refraction into the tunnel walls, to scattering by wall roughness, and to long range random tilt of the walls. Propagation around corners and through pillars is also examined based on a ray theory approach, together with the beneficial effects of placing reflectors at intersections to significantly reduce corner losses. The theory is found to be in fair agreement with the data; however, additional in-mine measurements are needed to provide a more conclusive test of the model.

17. Originator's Key Words	18. Availability Statement
Radio Propagation--UHF, Tunnels Tunnel Communications Mines--Radio Communication Mine Communication--Wireless Mines--Limestone, Coal	

19. U.S. Security Classif. of the Report	20. U.S. Security Classif. of This Page	21. No. of Pages	22. Price
		42	

PROPAGATION OF UHF RADIO WAVES IN LIMESTONE ROOM AND PILLAR MINES

Robert L. Lagace - Task Leader

Alfred G. Emslie

ARTHUR D. LITTLE, INC.

Cambridge, Massachusetts 02140

C-81863

The views and conclusions contained in this document are those of the authors and should not be interpreted as necessarily representing the official policies or recommendations of the Interior Department's Bureau of Mines or of the U. S. Government.

SUMMARY REPORT

USBM TASK ORDER NO. J0387217

Under Basic Agreement J0377065

JANUARY 1979

UNITED STATES
DEPARTMENT OF THE INTERIOR
BUREAU OF MINES

FOREWORD

This report was prepared by Arthur D. Little, Inc., Cambridge, Massachusetts, under USBM Task Order No. JO387217 under Basic Agreement JO377065. The contract was initiated under the Coal Mine Health and Safety Program. It was administered under the technical direction of the Pittsburgh Mining and Safety Research Center with Mr. Harry Dobroski acting as the technical project officer. Mr. Joseph Gilchrist was the contract administrator for the Bureau of Mines.

This report is a summary of the work recently completed as part of this contract during the period April 1978 to January 1979. This report was submitted by the authors in January 1979.

No inventions or patents were developed, and no applications for inventions or patents are pending.

TABLE OF CONTENTS

LIST OF TABLES

LIST OF FIGURES

I. INTRODUCTION

This report presents a mathematical model for the propagation of UHF radio waves in the tunnels of a room and pillar limestone mine, and describes the analysis of a small amount of propagation data obtained by R. L. Chufo and R. A. Isberg[1,2,3] in the Black River limestone mine in Kentucky. The model and analysis is based on the waveguide mode theory[4] developed earlier for the transmission of UHF waves in coal mine tunnels, with allowance for propagation losses due to refraction into the tunnel walls, to scattering by wall roughness, and to long range random tilt of the walls.

Two types of tunnel in the limestone mine are considered. One is a haulageway, containing a belt conveyor but no crosscuts, and having cross-sectional dimensions of about 20 ft. x 9 ft., which are comparable with the dimensions of the high-coal tunnels previously studied. The other kind of limestone tunnel occurs in a room and pillar area and has much larger cross-sectional dimensions, namely, 40 ft. wide by 35 ft. high. Each side wall of this large tunnel has an average open area of more than 50% owing to the presence of intersecting cross-cuts. A sample of the room and pillar geometry is shown in Figure 1, a plan view of a section of the mine.

The basic elements of the model are developed in the discussion of the haulageway tunnel, and then applied to the analysis of first the haulageway tunnel data and second the room and pillar area data. Propagation around corners and through pillars is also examined based on a ray theory approach, together with the beneficial effects of placing reflectors at intersections to significantly reduce corner losses. The theory is found to be in fair agreement with the data; however, additional in-mine measurements are needed to provide a more conclusive test of the model.

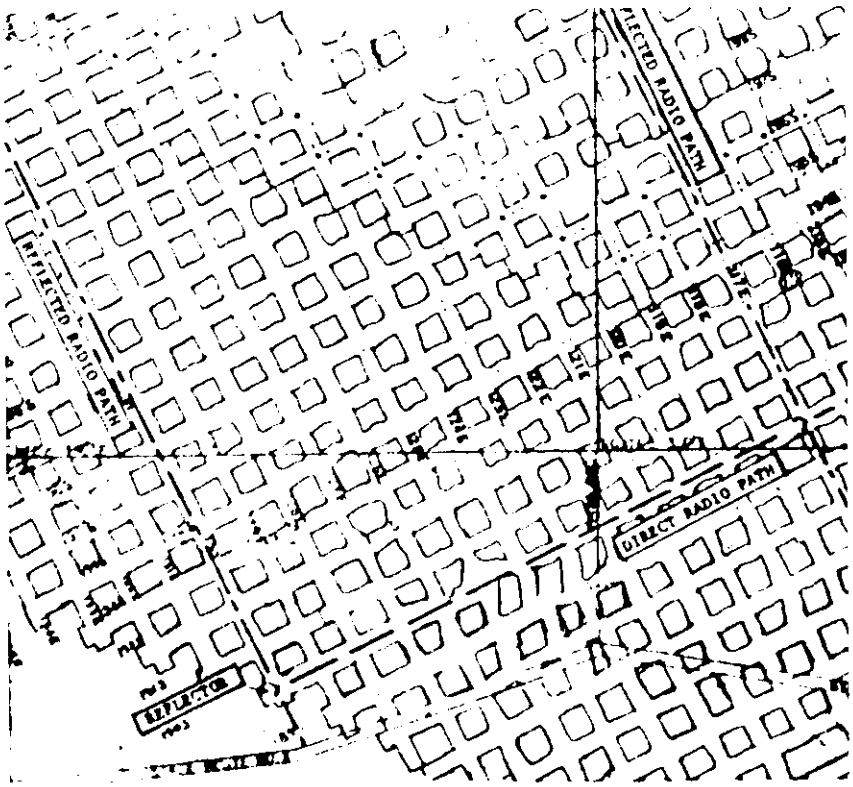

Source: Reference 1.

FIGURE 1 SECTIONS OF A PLAN VIEW MINE MAP OF A ROOM AND PILLAR LIMESTONE MINE

II. MODEL FOR HAULAGEWAY TUNNEL WITH BELT CONVEYOR

Figure 2 shows experimental data taken by Chufo and Isberg[1] of total signal attenuation in dB experienced along a small cross-section haulage tunnel at the two UHF frequencies of 466 MHz and 812 MHz. Figure 3 is a photograph depicting the actual tunnel environment. The total path attenuation is normalized with respect to isotropic transmitting and receiving antennas. Also shown for comparison are calculated free-space attenuation curves for the same frequencies. It is seen that the experimental data agree with the free-space curves at small ranges, but decay more rapidly at larger ranges. Beyond about 300 feet, however, the average trend is linear, which means that the electric field falls off exponentially with range in this region, rather than according to the free-space law.

We interpret this behavior in terms of excitation of the waveguide modes of the tunnel in the following way. The transmitting antenna excites a large number of these modes which decay exponentially with range at greatly different rates, depending on the horizontal and vertical mode number components n_1 and n_2. Theory shows[4] that the loss rate in dB/100 ft. is proportional to a linear combination of n_1^2, and n_2^2. Theory also shows that, if the width of the tunnel is greater than its height, as in the present haulageway case, the mode of smallest attenuation rate is the (1,1) mode with horizontal polarization, which we designate as $E_{h,1,1}$. We therefore postulate that, beyond a distance of about 300 feet, the only surviving mode is $E_{h,1,1}$.

A further postulate is necessary since the actual transmitting antenna, rather than being isotropic, is a vertical dipole. Such an antenna would not excite the $E_{h,1,1}$ mode of a smooth-walled tunnel. It has been found[5] experimentally, however, that at large ranges the polarization is predominantly horizontal no matter what the orientation of the transmitting antenna may be. We therefore assume that the tunnel walls are not ideally flat and smooth but have enough roughness and tilt to cause mode conversion from the initial vertically-polarized

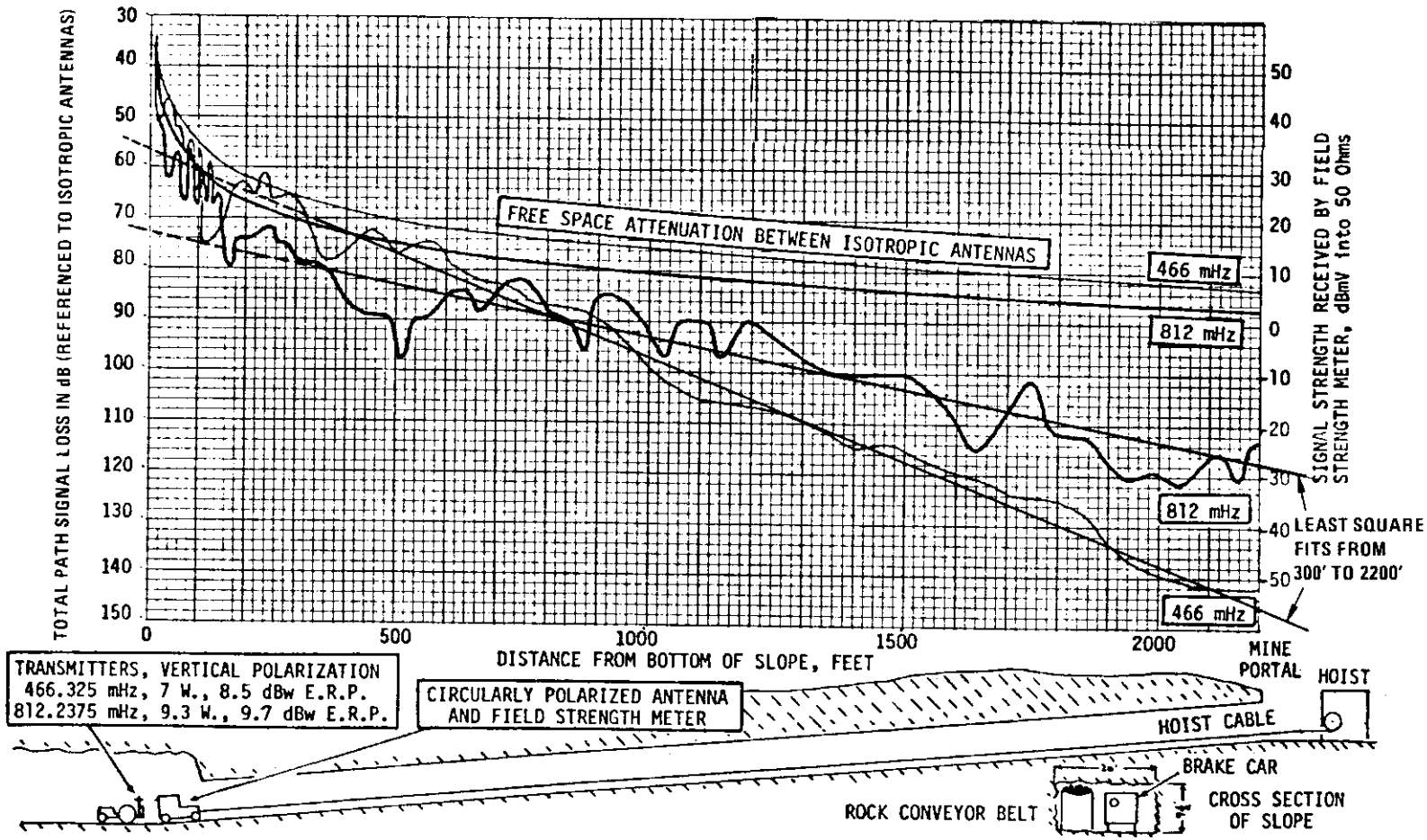

Source: Reference 1.

FIGURE 2 COMPARISON OF FREE SPACE LOSS AND MEASURED TOTAL PATH LOSS AT 466 AND 812 MHz IN BELT HAULAGEWAY OF BLACK RIVER LIMESTONE MINE

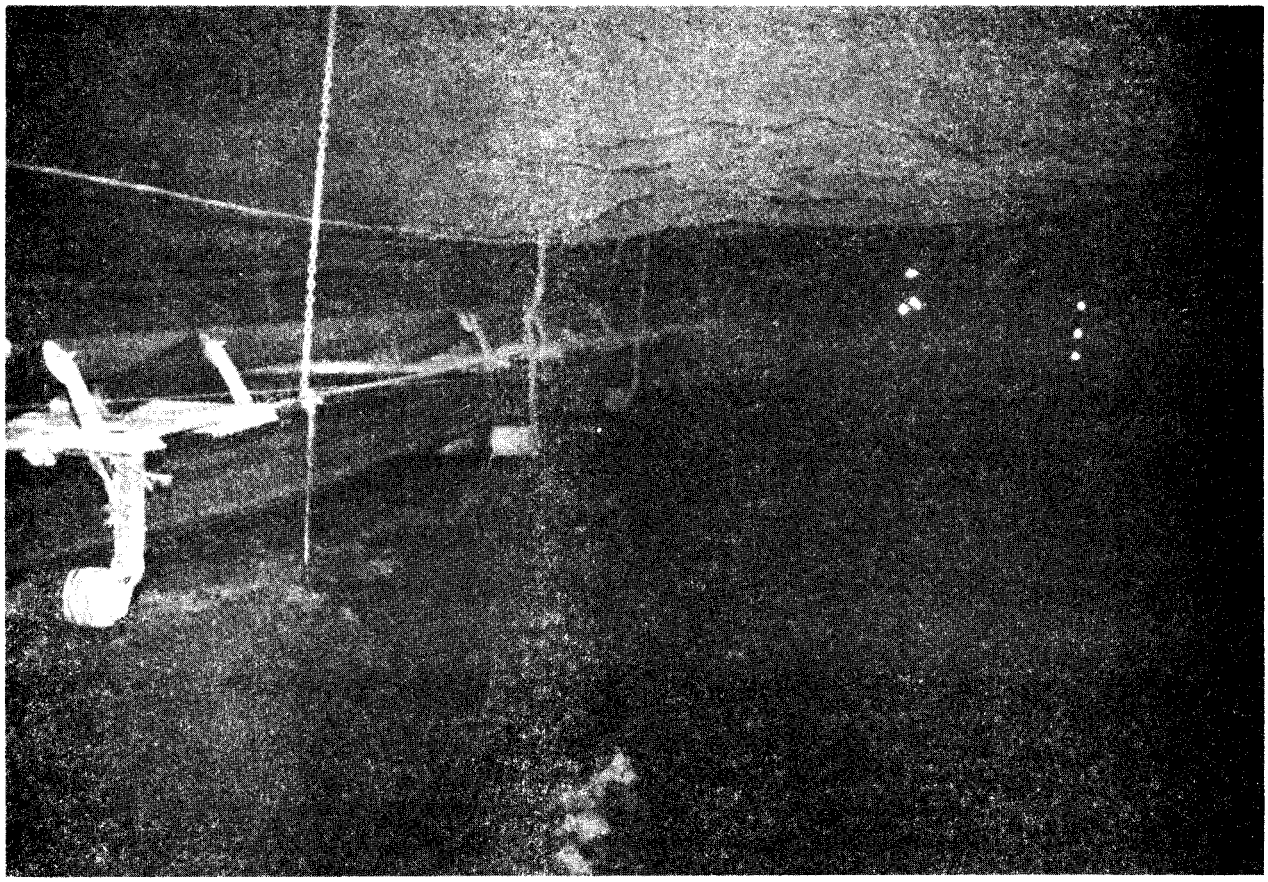

Source: U.S. Bureau of Mines.

FIGURE 3 PHOTOGRAPH OF HAULAGEWAY TUNNEL WITH BELT CONVEYOR IN LIMESTONE MINE

$E_{v,1,1}$ mode to the horizontally-polarized $E_{h,1,1}$ mode, within a distance of the order of 300 feet.

The first step in analyzing the data in Figure 2 is to determine the attenuation rate of the $E_{h,1,1}$ mode. To do this we fit a least-square straight line to the data from 300 to 2200 feet for each frequency. The two straight lines are shown in Figure 2. Table I gives the values of the attenuation coefficient α in dB/100 ft.

TABLE I

ATTENUATION COEFFICIENTS (EXPERIMENTAL VALUES)
FOR THE HAULAGEWAY TUNNEL

f (MHz)	α (dB/100 ft.)
466	4.02
812	2.03

Next we compare these experimental values of α with theoretical values for the $E_{h,1,1}$ mode. Three kinds of loss contribute to α: refraction loss, scattering loss due to wall roughness, and scattering loss due to random long range wall tilt relative to the mean planes of the four walls. In calculating these losses we use a combination of wave theory and ray theory.

A. REFRACTION LOSS

Each tunnel waveguide mode can be described, from the ray theory point of view, as a bundle of parallel rays which are reflected successively by all four walls of the tunnel. The grazing angles of reflection (in radians) are given by the expressions:

$$\phi_1 = \frac{n_1 \lambda}{2d_1} \tag{1}$$

$$\phi_2 = \frac{n_2 \lambda}{2d_2} , \tag{2}$$

where the subscript 1 refers to the side walls and the subscript 2 refers to the roof and floor. Thus n_1, n_2 are the horizontal and vertical mode numbers respectively; d_1 and d_2 are the horizontal and vertical tunnel dimensions; and λ is the free space wavelength. Expressions (1) and (2) are the conditions for phase coherence of the multiply reflected rays with each other.

The power gain for a distance z can be written as

$$g = g_1 g_2 \ , \tag{3}$$

where g_1 is the gain for side wall reflections and g_2 for roof and floor reflections. In reality, the gains are less than unity, and thereby correspond to power losses per reflection. In general, for either the haulage tunnel or the room-and-pillar tunnels,

$$g_1 = (FR_1)^{N_1} \tag{4}$$

$$g_2 = R_2^{N_2} \ . \tag{5}$$

F is the effective fraction of <u>reflecting</u> surface on the side walls, allowing for cross-cuts or other nonreflecting areas. N_1 and N_2 are the number of bounces of a ray in a distance z, given by

$$N_1 = \frac{\phi_1 z}{d_1} \tag{6}$$

$$N_2 = \frac{\phi_2 z}{d_2} \ . \tag{7}$$

Lastly, the power reflectances R_1 and R_2 are given by the Fresnel formulas

$$R_{1,h} = \left\{ \frac{K\phi_1 - (\phi_1^2 + K - 1)^{1/2}}{K\phi_1 + (\phi_1^2 + K - 1)^{1/2}} \right\}^2 \tag{8}$$

$$R_{2,h} = \left\{ \frac{\phi_2 - (\phi_2^2 + K - 1)^{1/2}}{\phi_2 + (\phi_2^2 + K - 1)^{1/2}} \right\}^2 \tag{9}$$

$$R_{1,v} = \left\{ \frac{\phi_1 - (\phi_1^2 + K - 1)^{1/2}}{\phi_1 + (\phi_1^2 + K - 1)^{1/2}} \right\}^2 \tag{10}$$

$$R_{2,v} = \left\{ \frac{K\phi_2 - (\phi_2^2 + K - 1)^{1/2}}{K\phi_2 + (\phi_2^2 + K - 1)^{1/2}} \right\}^2 \tag{11}$$

where K is the dielectric constant of the wall material and the subscripts h and v signify horizontal and vertical polarization, respectively. These are approximate expressions which are certainly valid for the small values of ϕ_1 and ϕ_2 that pertain to the dominant modes.

Therefore the attenuation rate $\alpha_{\text{refraction}}$ is given by

$$\alpha_{\text{refraction}} = -100\left(\frac{10 \log_{10} g}{Z}\right) \tag{12}$$

$$\alpha_{\text{refraction}} = -1000 \left[\frac{n_1 \lambda}{2d_1^2} \log_{10}(FR_1) + \frac{n_2 \lambda}{2d_2^2} \log_{10}(R_2) \right] \tag{13}$$

where λ, d_1, and d_2 are expressed in feet, and $\alpha_{\text{refraction}}$ in dB/100 ft.

B. ROUGHNESS LOSS

We assume as in Ref. 4, that the walls of the tunnel are rough, as illustrated in the close-up photograph of a sidewall in Figure 4, with a Gaussian amplitude distribution about the mean surface described by a root mean square value of h. The power loss factors per reflection are then given by

$$g_1 = e^{-2\left(\frac{2\pi h \sin\phi_1}{\lambda}\right)^2} \tag{14}$$

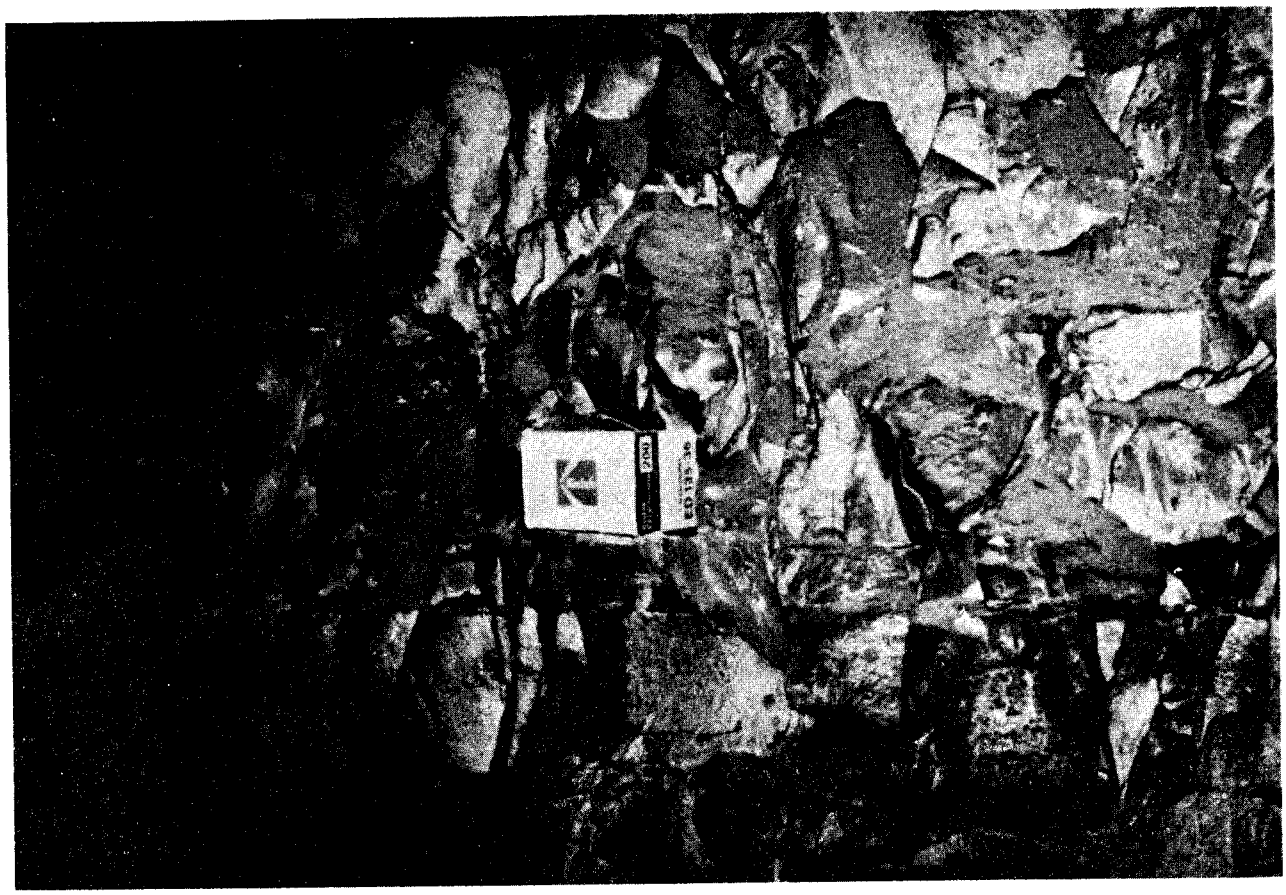

Source: U.S. Bureau of Mines.

FIGURE 4 CLOSE-UP PHOTOGRAPH ILLUSTRATING ROUGHNESS OF A SIDE WALL

$$g_2 = e^{-2\left(\frac{2\pi h \sin\phi_2}{\lambda}\right)^2} \tag{15}$$

Again taking ϕ_1 and ϕ_2 as small angles, we find, from (1), (2), (3), (6), and (7) that the attenuation rate due to roughness is

$$\alpha_{\text{roughness}} = 434.3\ \pi^2 h^2 \lambda \left(\frac{n_1^3}{n_1^4} + \frac{n_2^3}{d_2^4}\right) \tag{16}$$

where all lengths are in feet and $\alpha_{\text{roughness}}$ is in dB/100 ft.

C. TILT LOSS

Instead of calculating the tilt loss for a fixed tilt angle θ_o, as in Ref. 4, we now consider the long range tilt to have a Gaussian distribution with a root mean square value θ_o (radians). For a particular reflection at a part of a side-wall where the tilt angle is θ, the reflected beam is inclined at an angle $\phi_1 + 2\theta$ with respect to the wall. The electric field of this beam therefore has the form

$$E' = E_o\ e^{-ik_o[Z\cos(\phi_1 + 2\theta) + x\sin(\phi_1 + 2\theta)]} \tag{17}$$

whereas the field of the mode is

$$E = E_o\ e^{-ik_o[Z\cos\phi_1 + x\sin\phi_1]} \tag{18}$$

where $k_o = 2\pi/\lambda$.

The power coupling factor of E' back into the mode E is given by the normalized overlap integral

$$g_1(\theta) = \frac{\left|\iint_E E'^*\, dxdy\right|^2}{\left(\iint |E|^2 dxdy\right)\left(\iint |E'|^2 dxdy\right)}\ , \tag{19}$$

where the integrations are taken over the cross-section of the tunnel. For small θ and ϕ_1 (17) reduces to

$$g_1(\theta) = \left(\frac{\sin k_o \theta d_1}{k_o \theta d_1}\right)^2 , \tag{20}$$

and likewise,

$$g_2(\theta) = \left(\frac{\sin k_o \theta d_2}{k_o \theta d_2}\right)^2 . \tag{21}$$

We now introduce the statistics by using the Gaussian weighting factor

$$p(\theta) = \frac{1}{\theta_o \sqrt{2\pi}} \; e^{-\theta^2/2\theta_o^2} . \tag{22}$$

Then

$$g_1 = \int_{-\infty}^{\infty} g_1(\theta) \; p(\theta) \; d\theta \tag{23}$$

$$g_2 = \int_{-\infty}^{\infty} g_2(\theta) \; p(\theta) \; d\theta \tag{24}$$

In order to avoid numerical integration, we use the approximation

$$\left(\frac{\sin x}{x}\right)^2 \approx e^{-x^2/3} , \tag{25}$$

and obtain for (21) and (22) the closed form expressions:

$$g_1 \cong \frac{1}{\left[1 + \frac{2}{3}\left(\frac{2\pi\theta_o d_1}{\lambda}\right)^2\right]^{1/2}} \tag{26}$$

$$g_2 \cong \frac{1}{\left[1 + \frac{2}{3}\left(\frac{2\pi\theta_o d_2}{\lambda}\right)^2\right]^{1/2}} \tag{27}$$

Then from (1), (2), and (3), the tilt loss rate becomes:

$$\alpha_{tilt} = -\frac{500n_1\lambda}{d_1^2}\log_{10}g_1 - \frac{500n_2\lambda}{d_2^2}\log_{10}g_2 \qquad (28)$$

where all lengths are in feet and α_{tilt} in dB/100 ft.

D. COMPARISON OF THEORY WITH HAULAGE TUNNEL DATA

The haulage tunnel has nominal dimensions of 20 ft. in width and 9.5 ft. in height. However, Figure 2 and the photograph of Figure 3 indicate that the conveyor belt system occupies about 5 ft. of the width and contains equipment and debris that would trap incident UHF waves. We therefore assume that the effective dimensions of the tunnel are d_1 = 15 ft. and d_2 = 9.5 ft., and that only a fraction 2/3 of the area of the wall on the conveyor-belt side is reflecting. This means that the geometric mean of the reflecting fractions of the two side walls is $F = (2/3 \times 1)^{1/2} = 0.816$. The wavelengths corresponding to the frequencies of 466 MHz and 812 MHz used in the experiments are λ = 2.11 ft. and 1.21 ft., respectively. The dielectric constant K of limestone is assumed to be 5. Moderate errors in this assumed value are tolerable, since calculations show that the final results are very insensitive to K.

For these values of the physical constants Eq (13) gives the values of $\alpha_{refraction}$ shown in Table II, for both the $E_{h,1,1}$ and $E_{v,1,1}$ modes.

TABLE II

COMPARISON OF THEORETICAL $\alpha_{refraction}$ WITH EXPERIMENTAL α_{total} FOR HAULAGE TUNNEL

f (MHz)	Theoretical $\alpha_{h,refr.}$ (dB/100')	Theoretical $\alpha_{v,refr.}$ (dB/100')	Experimental α_{total} (dB/100')
466	3.60	7.12	4.02
812	1.43	2.57	2.03

It is seen that the $E_{h,1,1}$ values for $\alpha_{refraction}$ are comparable with the experimentally determined α_{total} results, although somewhat lower. This is reasonable since roughness and tilt losses have not yet been included. The $E_{v,1,1}$ values are definitely higher than the experimental values, in accord with the idea that the horizontally polarized (1,1) mode always dominates at large distances for tunnels of this shape.

If we now include the roughness and tilt effects, we find from a series of trial calculations, using Eq (16) and (28), that roughness and tilt values h = 0.2 ft. and θ_o = 0.0122 radian = 0.7°, give good agreement between theory and experiment as shown in Table III.

TABLE III

COMPARISON OF THEORETICAL α_{total} FOR $E_{h,1,1}$ MODE WITH EXPERIMENTAL α_{total} FOR HAULAGE TUNNEL FOR h = 0.2 FT. AND θ_o = 0.122 RADIAN = 0.7°

f (MHz)	$\alpha_{refr.}$ (dB/100')	$\alpha_{roughness}$ (dB/100')	α_{tilt} (dB/100')	α_{total} (dB/100')	α_{expt} (dB/100')
466	3.60	0.051	0.377	4.03	4.02
812	1.43	0.029	0.589	2.05	2.03

E. MODE CONVERSION

Since the transmitting antenna in the haulage tunnel is a vertical dipole, whereas the received signal at large distances is mainly the $E_{h,1,1}$ mode, the structure of the tunnel walls must be such as to cause mode conversion from the $E_{v,1,1}$ and higher order vertically polarized modes to the $E_{h,1,1}$ mode. This conversion process clearly requires that portions of the tunnel walls are tilted about the longitudinal z-axis of the tunnel, or that conductors with this kind of tilt are present in the tunnel. The support structure of the conveyor belt indeed contains metal struts and other members oriented in this way as shown in Figure 3.

The vertically-polarized mode having, by far, the greatest coupling to the $E_{h,1,1}$ mode is the $E_{v,1,1}$ mode. The reason is that these two modes have exactly the same spatial structure, of the form $\cos(\pi x/d_1)\cos(\pi y/d_2)$, whereas higher modes are orthogonal to the $E_{h,1,1}$ mode. We therefore consider only the interaction between the two (1,1) modes, which can be described by means of the following coupled differential equations:

$$\frac{dI_h}{dz} = - a_h I_h - a_{hv} I_h + a_{vh} I_v \tag{29}$$

$$\frac{dI_v}{dz} = - a_v I_v - a_{vh} I_v + a_{hv} I_h \tag{30}$$

where I_h, I_v are the intensities of the two waves, a_h and a_v are the power attenuation coefficients, and a_{vh}, a_{hv} are the power coupling constants of the waves. From the reciprocity principle it follows that

$$a_{vh} = a_{hv} \, . \tag{31}$$

Equations (29) and (30) can be written in the more compact form

$$\frac{dI_h}{dz} = -a_1 I_h + a_{12} I_v \tag{32}$$

$$\frac{dI_v}{dz} = -a_2 I_v + a_{12} I_h \tag{33}$$

where

$$a_1 = a_h + a_{hv} \tag{34}$$

$$a_2 = a_v + a_{hv} \tag{35}$$

$$a_{12} = a_{hv} \tag{36}$$

The solution of (32) and (33) for the boundary conditions $I_h = 0$, $I_v = I_o$ at $z = 0$, is

$$I_h = \frac{a_{12} I_o}{\lambda_+ - \lambda_-} \left(e^{-\lambda_- z} - e^{-\lambda_+ z} \right) \tag{37}$$

$$I_v = \frac{I_o}{\lambda_+ - \lambda_-} \left[(a_1 - \lambda_-) e^{-\lambda_- z} - (a_1 - \lambda_+) e^{-\lambda_+ z} \right], \tag{38}$$

where

$$\lambda_+ = \frac{1}{2} \left[a_1 + a_2 + \sqrt{(a_1 + a_2)^2 - 4\left(a_1 a_2 - a_{12}^2\right)} \right] \tag{39}$$

$$\lambda_- = \frac{1}{2} \left[a_1 + a_2 - \sqrt{(a_1 + a_2)^2 - 4\left(a_1 a_2 - a_{12}^2\right)} \right]. \tag{40}$$

From (39), (40), (34), and (35),

$$\lambda_+ - \lambda_- = \sqrt{(a_v - a_h)^2 + 4a_{vh}^2} \tag{41}$$

If we make the reasonable assumption that a_{vh} is small compared with $a_v - a_h$, Eq (37) becomes

$$I_h \approx I_o \frac{a_{vh}}{a_v - a_h} \left(e^{-a_h z} - e^{-a_v z} \right) \tag{42}$$

This shows that I_h reaches a maximum at the distance

$$z_m = \frac{\ell n \left(\frac{a_v}{a_h} \right)}{a_v - a_h} \tag{43}$$

From Table II we find, on considering only the refraction losses and converting from dB/100 ft. to $(\text{ft.})^{-1}$, that a_h and a_v have the values .0083 ft.^{-1} and .0164 ft.^{-1} at 466 MHz, and the values .0033 ft.^{-1} and .0059 ft.^{-1} at 812 MHz, respectively. Therefore, upon substitution of these a_v and a_h values into (43), we get z_m = 84 ft. at 466 MHz and 223 ft. at 812 MHz. These results are consistent with the point on Figure 2 at about 300 ft. beyond which exponential decay takes over. Inclusion of roughness and tilt losses would reduce z_m somewhat.

For large values of z, (37) and (38) reduce to the approximate forms:

$$I_h \approx I_o \left(\frac{a_{vh}}{a_v - a_h} \right) e^{-a_h z} \tag{44}$$

$$I_v \approx I_o \left(\frac{a_{vh}}{a_v - a_h} \right)^2 e^{-a_h z} \tag{45}$$

In these equations a_h and a_v can be calculated at each frequency from the roughness and tilt parameters determined above. Also I_h versus z is known for large z from the experimental data. However, I_v versus z at large z is not known experimentally from the measurements to date in the belt haulageway. Therefore Eq (45) does not provide any useful information for analyzing the current set of data. This means that we have two unknown quantities, namely, I_o and a_{vh} and only one equation, i.e., Eq (44). There is therefore not enough information in the present set of data to determine the mode conversion parameter a_{vh}.

If the unknown intensity I_o is eliminated from (44) and (45), we obtain the simple relation

$$\frac{I_v}{I_h} = \frac{a_{vh}}{a_v - a_h} \quad , \tag{46}$$

for the equilibrium ratio of the two (1,1) modes at large distances. This ratio could easily be determined by means of a dipole receiving antenna that could be oriented first vertically and then horizontally. Then (46) would permit the determination of a_{vh}.

III. APPLICATION TO TUNNELS IN ROOM AND PILLAR AREAS

A. COMPARISON OF THEORETICAL AND EXPERIMENTAL RESULTS

Figures 5 - 10 show the results of experiments on propagation around corners in a room and pillar area, with and without the help of a metal reflector having two perpendicular 4 ft. x 4 ft. panels mounted in an intersection near the roof and inclined at 45° to the two intersecting cross-cuts as shown in Figure 11. In each graph the vertical scale represents the received signal in dB relative to 1 μV. Also included in each figure is a diagram showing the relative positions of the fixed receiver, the corner, and the movable transmitter.

Figures 5 and 6 show that a marked decrease in signal loss rate occurs beyond the corner when the reflector is located at the intersection of the two tunnels containing the transmitter and receiver. In discussing the result it is convenient to consider the transmitter and receiver to be interchanged, which makes no difference to the signal, according to the reciprocity principle. Then the TX dipole now replacing the RX dipole at the bottom of the diagram in Figure 5 excites many modes of the tunnel which attenuate at very different rates depending on the mode numbers n_1 and n_2. By the time the waves reach the corner, 1300 feet away, only the two (1,1) modes have appreciable amplitude. These modes are very well collimated since the grazing mode angles ϕ_1 and ϕ_2 are of the order of 1°. The portion of the wave that enters the aperture of the cross tunnel is therefore very small, and furthermore is nearly pependicular to the cross-tunnel side walls. The modes excited in the cross tunnel are therefore high-order modes which decay rapidly, in agreement with Figure 5. On the other hand when a reflector is present at the corner, a substantial fraction of each incident (1,1) mode is re-directed down the cross tunnel, and preferentially excites low order modes in the cross tunnel, which decay at a lower rate, as in Figure 6.

In order to check these arguments we show on Figures 5 and 6 the theoretical decay rate of the $E_{h,1,1}$ mode calculated for K = 5 and the

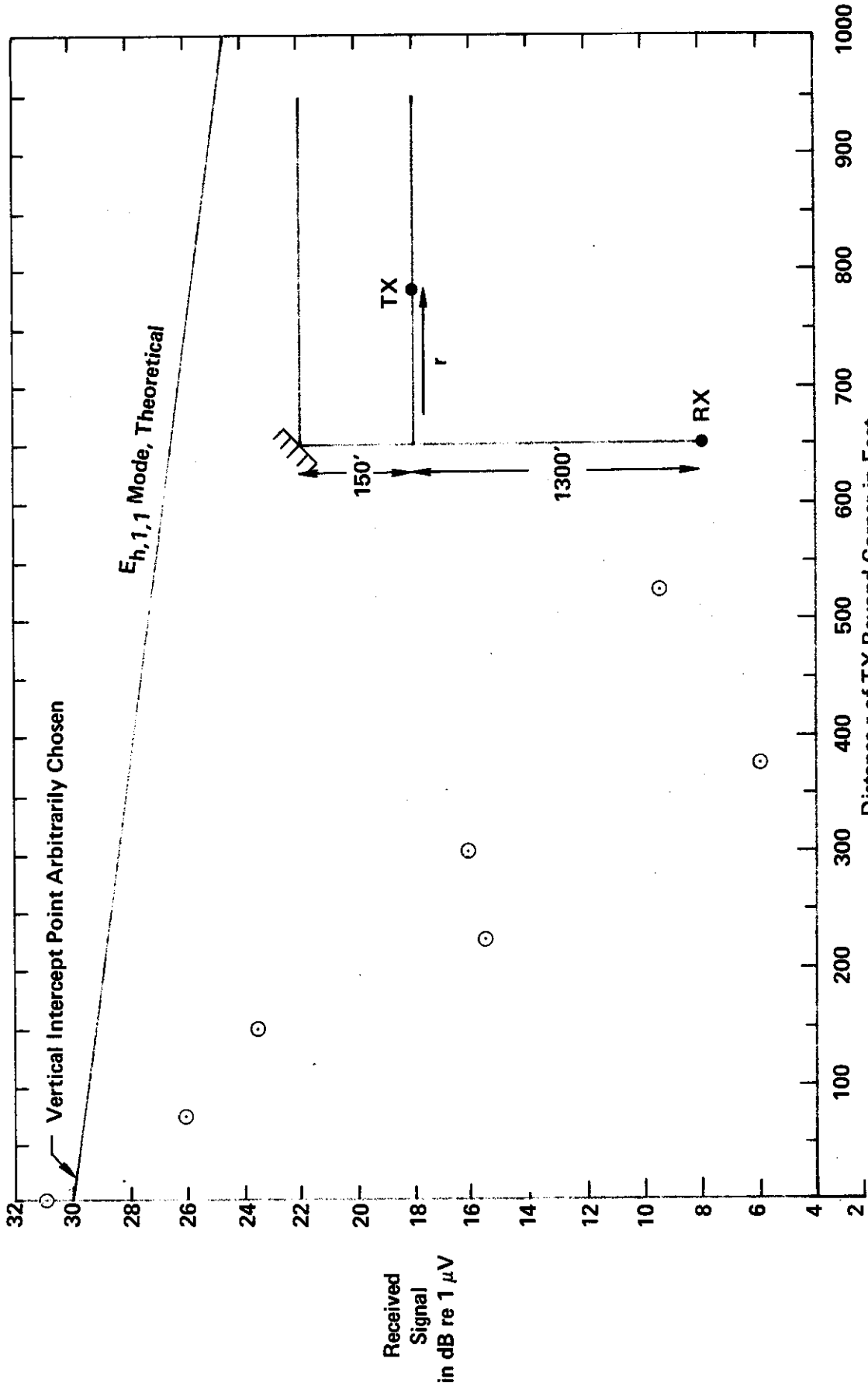

Source: Reference 1, Figure 7.

FIGURE 5 SIGNAL STRENGTH VERSUS DISTANCE AROUND A CORNER HAVING NO REFLECTOR – f = 466 MHz – GEOMETRY A

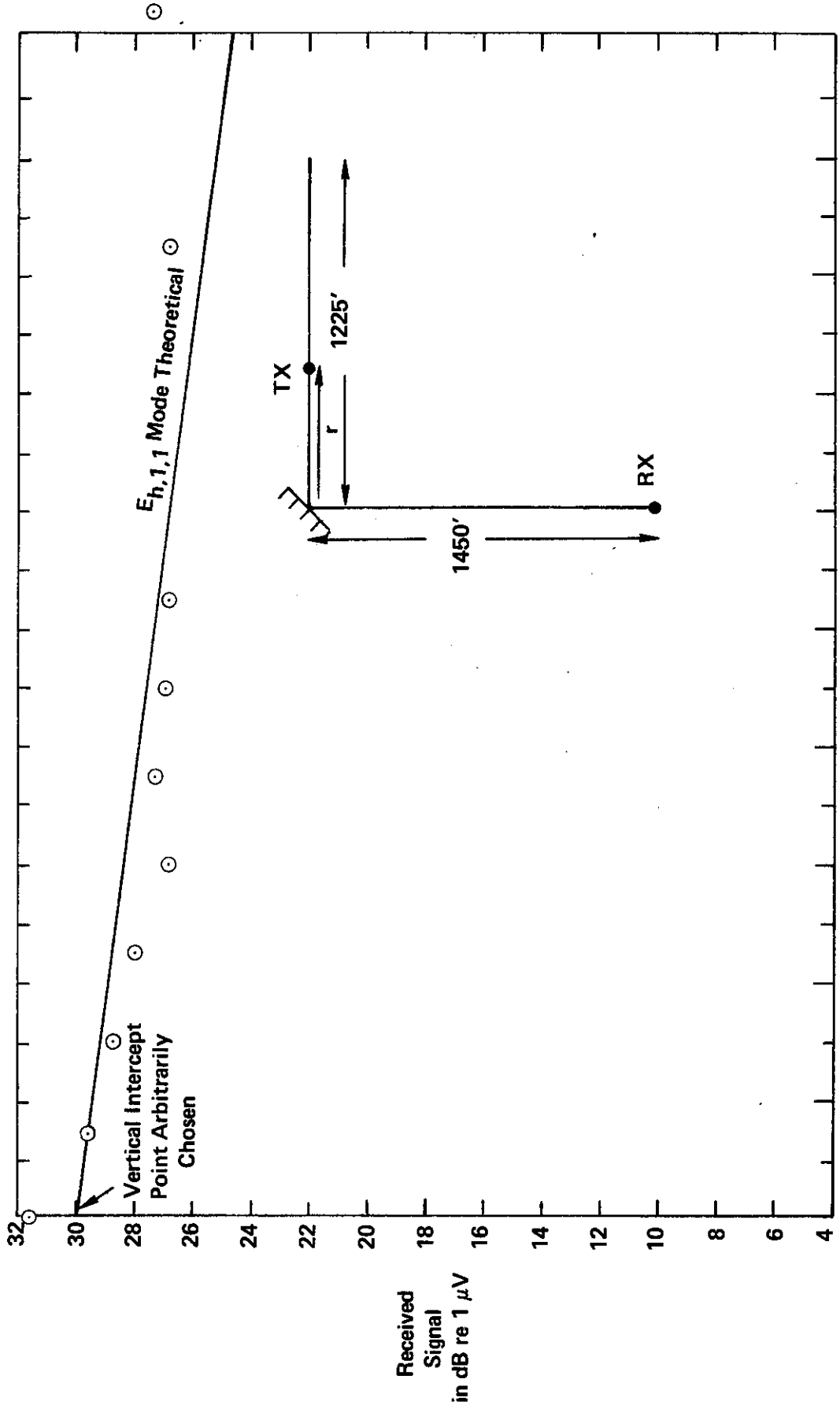

Source: Reference 1, Figure 7.

FIGURE 6 SIGNAL STRENGTH VERSUS DISTANCE AROUND A CORNER HAVING A REFLECTOR – f = 466 MHz – GEOMETRY B

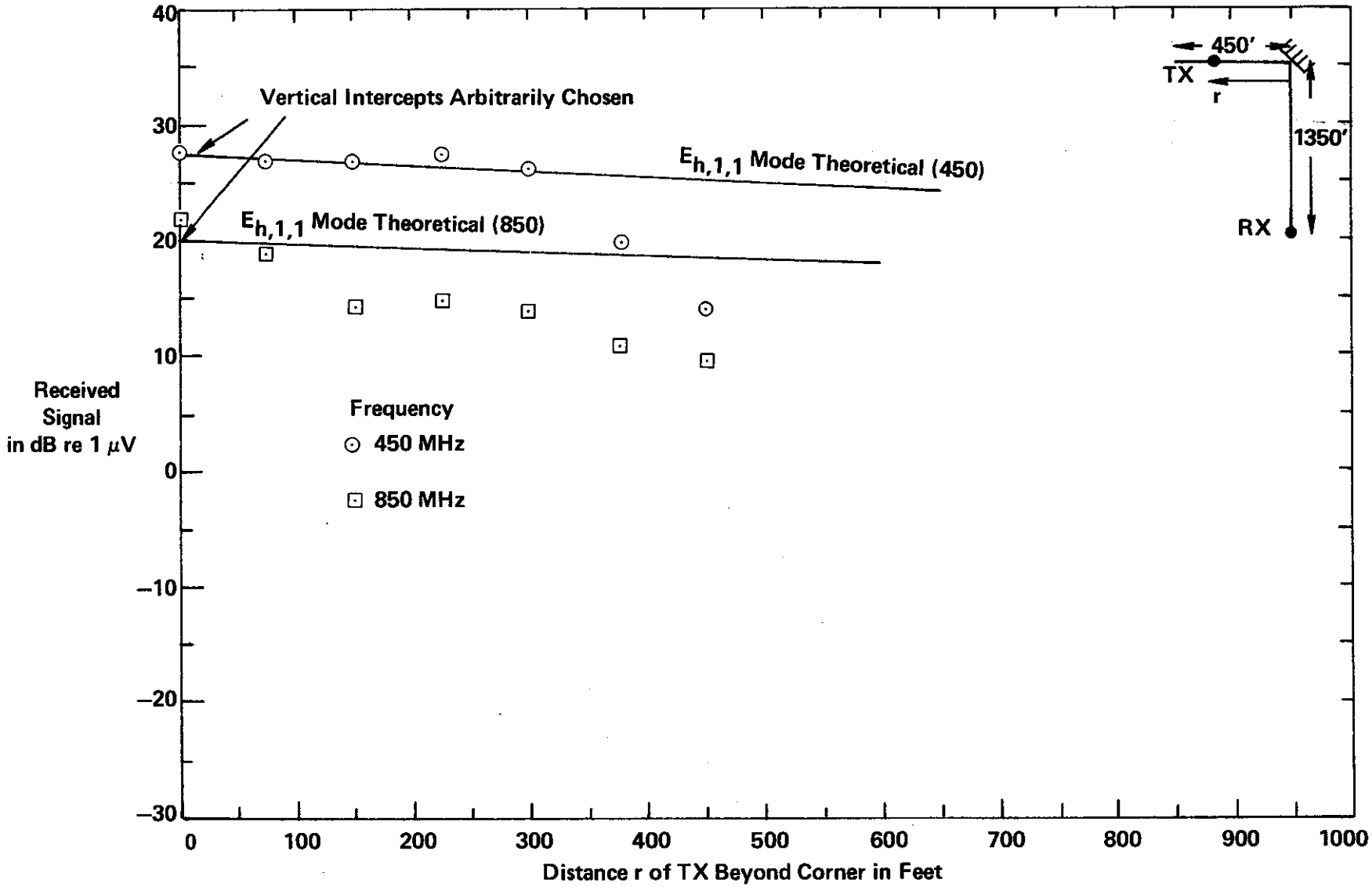

Source: Reference 4.

FIGURE 7 SIGNAL STRENGTH VERSUS DISTANCE AROUND A CORNER WITH A REFLECTOR AT 450 MHz AND 850 MHz – GEOMETRY C

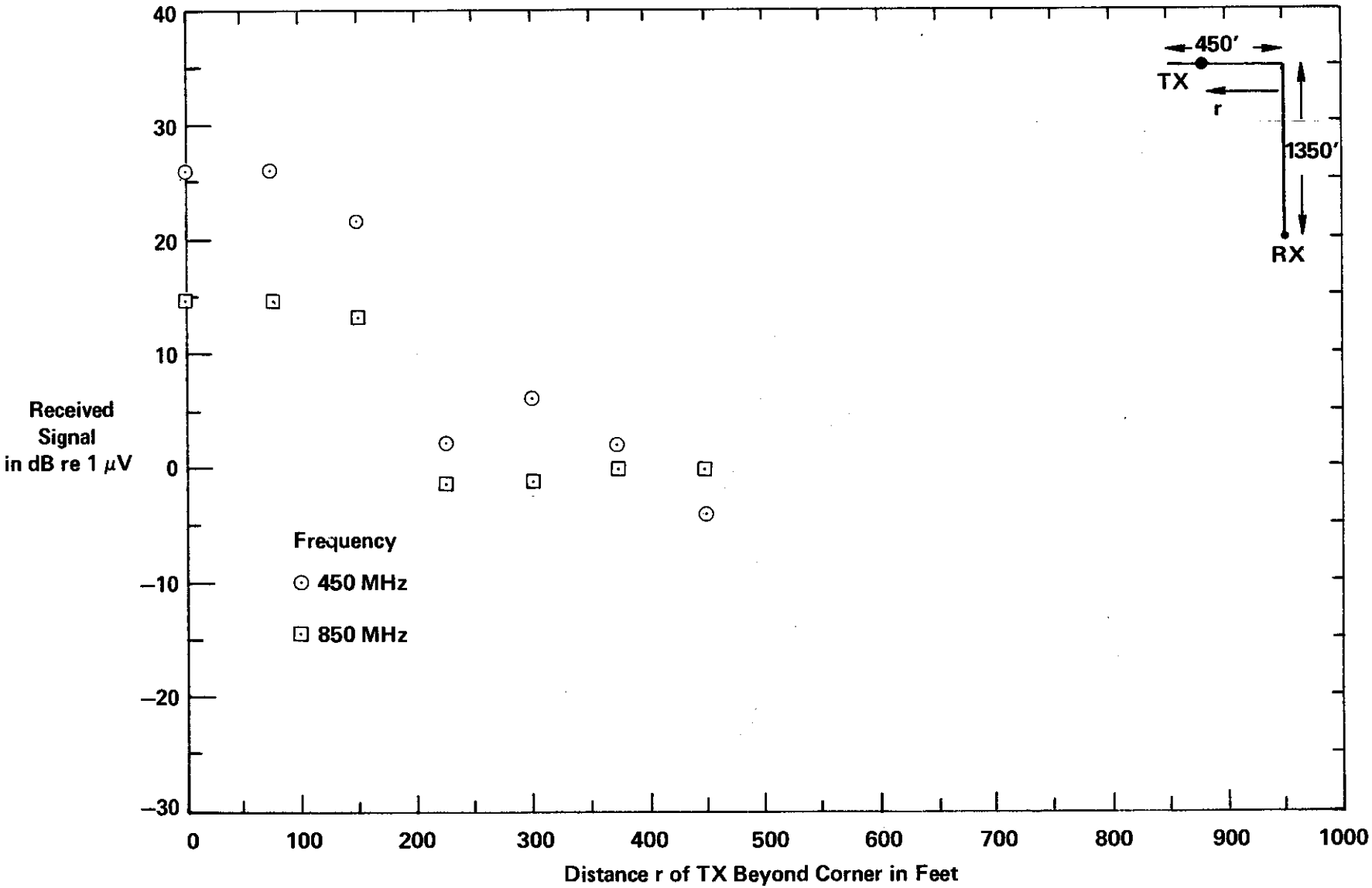

Source: Reference 3.

FIGURE 8 SIGNAL STRENGTH VERSUS DISTANCE AROUND A CORNER WITHOUT A REFLECTOR AT 450 AND 850 MHz — GEOMETRY C

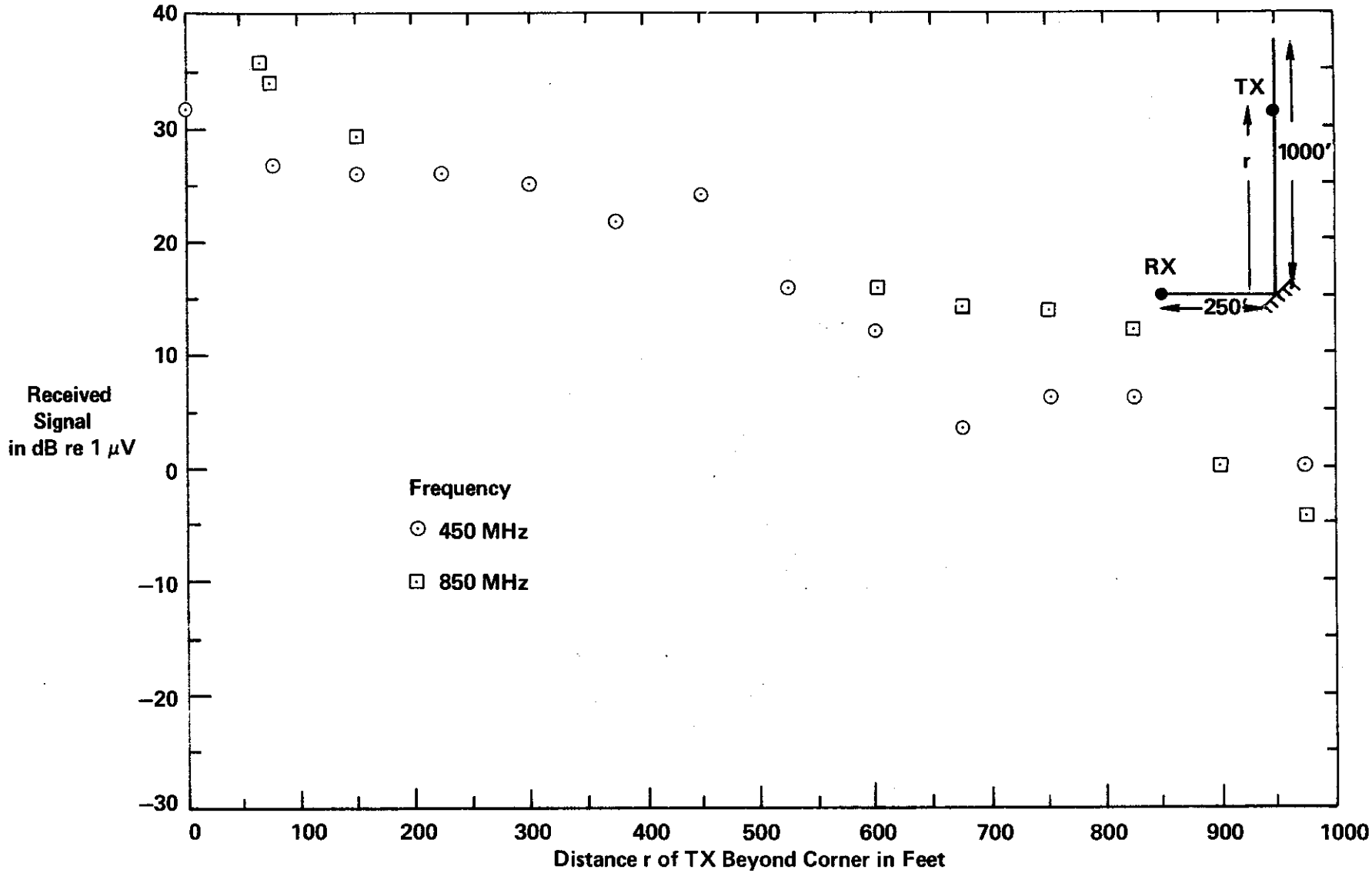

Source: Reference 3.

FIGURE 9 SIGNAL STRENGTH VERSUS DISTANCE AROUND A CORNER WITH A REFLECTOR AT 450 AND 850 MHz – GEOMETRY D

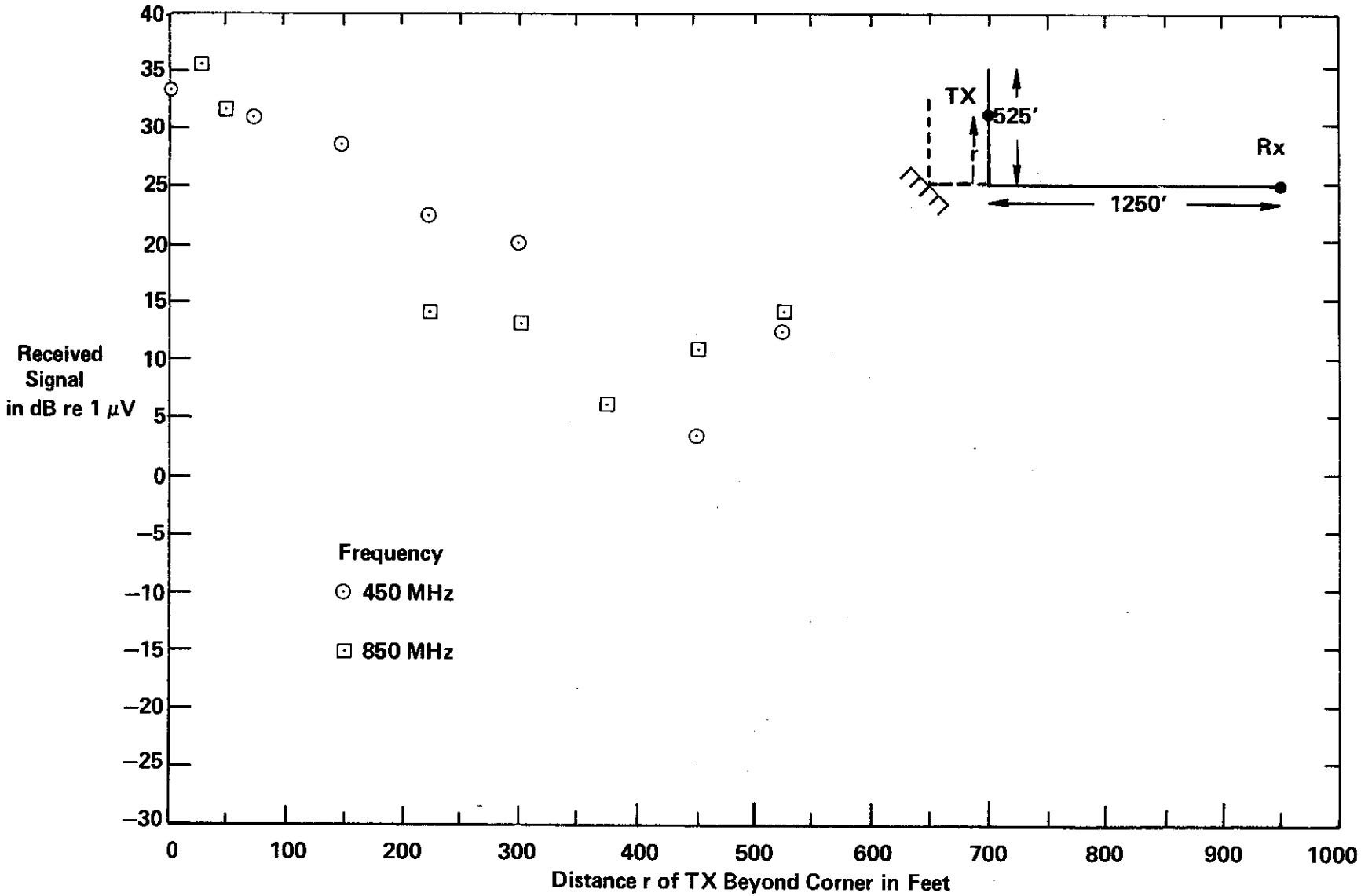

Source: Reference 3.

FIGURE 10 SIGNAL STRENGTH VERSUS DISTANCE AROUND A CORNER WITHOUT A REFLECTOR AT 450 AND 850 MHz – GEOMETRY E

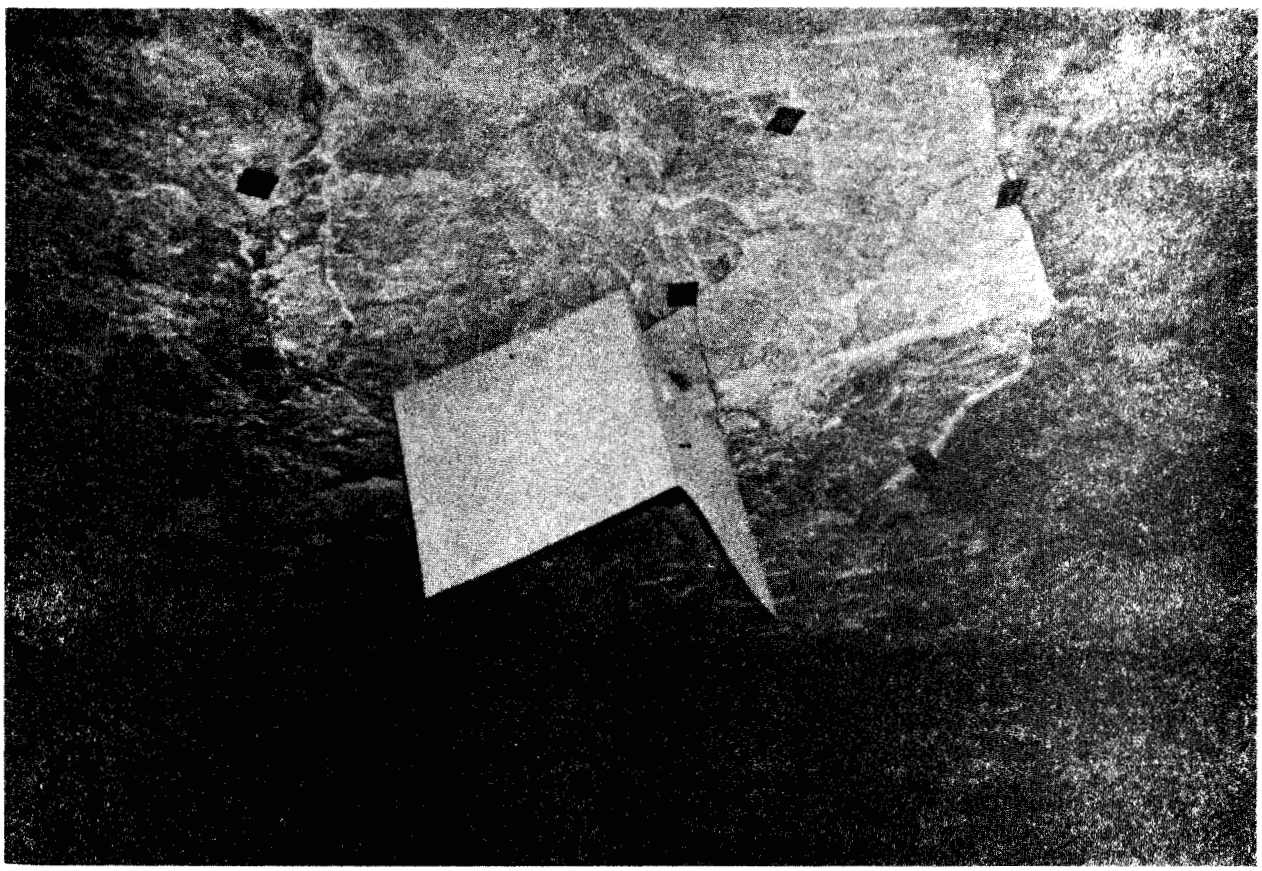

Source: U.S. Bureau of Mines

FIGURE 11 METAL REFLECTORS MOUNTED NEAR THE ROOF IN AN INTERSECTION OF TWO TUNNELS IN A LIMESTONE MINE

same roughness and tilt values, h = 0.2 ft. and θ_o = 0.0122 radian = 0.7° found for the haulage tunnel. However, we use tunnel dimensions of d_1 = 40 ft. and d_2 = 35 ft., and a value F = 0.467 which corresponds to the 35 to 40 ratio of reflecting area to open area on the side walls of the tunnel in the room and pillar area. For these parameters, the theory gives loss rates of 0.53 dB/100 ft. for the $E_{h,1,1}$ mode and 0.56 dB/100 ft. for the $E_{v,1,1}$ mode, at 466 MHz. The near equality of the two loss rates is due to the almost square cross-section of the tunnel. The vertical positions of the $E_{h,1,1}$ theoretical curves in Figures 5 and 6 are arbitrarily chosen. It is seen that the slope of the line agrees fairly well with the experimental points in Figure 6. In addition, the period of the oscillatory character of the experimental points suggests interference between the $E_{h,1,1}$ and $E_{v,1,1}$ modes, which are close in amplitude and phase velocity. However, it is not clear how a vertical receiving antenna would sense this.

In Figure 7 (with-reflector) the calculated theoretical $E_{h,1,1}$ curves for 450 and 850 MHz do not agree very well with most of the experimental points at these frequencies. In Figure 8 (without reflector) the experimental decay rates are greater than those in Figure 7, but not as markedly different as in the cases of Figures 5 and 6. The reason for this is not very clear. In Figure 9, with a reflector at the corner, the experimental decay rates show signs of interference, but the rates seem to be much greater than the theoretical $E_{h,1,1}$ and $E_{v,1,1}$ rates. Figure 10, with no reflector at the corner, shows experimental decay rates considerably greater than in Figure 9, as expected.

The reason for the high experimental attenuation rates relative to the calculated $E_{h,1,1}$ values may be that the higher modes have not completely died out in distances of the order of 1000 feet around the corner. Table IV gives calculated values of the attenuation constants α_h and α_v for a number of higher modes at 450 MHz, for the same parameters as before. It is seen that for a 1000 foot distance the total attenuation is about 7 dB for the (1,1) modes, 16 dB for the (2,2)

TABLE IV

THEORETICAL ATTENUATION RATES OF LOWEST AND HIGHER ORDER MODES AT 450 MHz FOR TUNNEL IN ROOM AND PILLAR AREA FOR d_1 = 40 FT., d_2 = 35 FT., F = 0.467, K = 5, h = 0.2 FT. θ_o = 0.0122 RADIAN = 0.7°

Mode No.'s		Refraction		Roughness	Tilt	Total	
n_1	n_2	α_h (dB/100')	α_v (dB/100')	α_h, α_v (dB/100')	α_h, α_v (dB/100')	α_h (dB/100')	α_v (dB/100')
1	1	0.399	0.430	0.0004	.259	0.658	0.689
1	2	0.765	1.088	.0021	.393	1.160	1.483
2	1	0.644	0.479	.0014	.383	1.028	0.863
2	2	1.009	1.136	.0032	.517	1.558	1.656
1	3	1.178	1.997	.0068	.528	1.713	2.532
3	1	1.057	0.560	.0042	.507	1.568	1.071
2	3	1.423	2.046	.0079	.652	2.083	2.706
3	2	1.423	1.217	.0059	.642	2.071	1.865
3	3	1.836	2.127	.0106	.776	2.623	2.914
1	4	1.640	3.175	.0160	.662	2.318	3.853
4	1	1.646	0.673	.0096	.631	2.287	1.314
2	4	1.885	3.223	.0170	.786	2.688	4.026
4	2	2.012	1.331	.0113	.766	2.789	2.108
3	4	2.298	3.304	.0198	.910	3.228	4.234
4	3	2.425	2.240	.0160	.900	3.341	2.272
4	4	2.887	3.418	.0252	1.035	3.947	4.478

modes, and 28 dB for the (3,3) modes. Thus the higher modes do die out fairly rapidly compared with the (1,1) modes. However, beats between the two (1,1) modes will persist for quite large distances.

B. PREDICTED VARIATION OF ATTENUATION RATE OF (1,1) MODES WITH FREQUENCY

Table V shows how the attenuation rates of the (1,1) modes vary with frequency, again for the same parameters. As expected for tunnels having nearly equal vertical and cross-sectional dimensions, the vertical and horizontal attenuation rates are also close in value. The total attenuation rates are seen to fall steadily with increasing frequency, which suggests that microwave frequencies would be worth trying, especially since reflectors at the tunnel intersections would have much sharper reflected main beam patterns, and would therefore couple much more efficiently into the (1,1) modes of the cross-cut. Should this beam sharpening introduce a reflector alignment accuracy requirement at say X-band wavelengths, simply reducing the size of the reflector will broaden the beam to more tolerable widths. It is to be noted that roughness loss becomes negligible at high frequencies. An interesting prediction of the theory is that the tilt loss should at first increase with frequency, reach a broad maximum at about 1000 MHz, and then steadily decrease.

TABLE V

VARIATION OF THEORETICAL ATTENUATION RATES
WITH FREQUENCY FOR TUNNEL IN A ROOM AND PILLAR AREA
FOR $n_1 = n_2 = 1$, $d_1 \doteq 40$ FT., $d_2 = 35$ FT. $F = 0.467$
$K = 5$, $h = 0.2$ FT., $\theta_o = 0.0122$ RADIAN $= 0.7°$

Frequency f (MHz)	Refaction α_h (dB/100')	Refaction α_v (dB/100')	Roughness α_h, α_v (dB/100')	Tilt α_h, α_v (dB/100')	Total α_h (dB/100')	Total α_v (dB/100')
500	.349	.375	.00035	.269	.618	.642
1,000	.153	.160	.00018	.289	.442	.449
1,500	.098	.100	.00012	.267	.365	.367
2,000	.071	.073	.00009	.242	.313	.315
3,000	.046	.047	.00006	.201	.247	.248
5,000	.027	.028	.00004	.152	.179	.180
10,000	.013	.013	.00002	.097	.110	.110

IV. COMMENTS ON PROPAGATION IN A COAL MINE TUNNEL

Table VI shows calculated attenuation rates for the coal mine tunnel investigated in Reference 4, including revised values of the attenuation rate due to tilt, based on the improved tilt theory given in the present report. It is seen that, although α_{tilt} has a flat maximum at about 3000 MHz, α_{total} decreases steadily with increasing frequency, instead of falling to a minimum and then increasing as in Reference 4. It turns out, however, that the rms tilt angle $\theta_o = 1°$ used in the present calculation gives as good a fit to the original experimental data as the constant-θ value of 1° used in Reference 4. The results in Table VI suggest that even higher frequencies than 1000 MHz may be usable in coal mines as well as in limestone mines. However, one must keep in mind that the attenuation rates in tunnels having large scale undulations (like in some coal seams) that obstruct the line of sight will be more severely affected at the higher frequencies.

Although portable and mobile equipment are not commercially available above 1000 MHz, fixed point to point mine communication applications may arise that are suited to the use of available fixed station equipment at these higher frequencies. The use of small, compact, low power police radar equipment may be well suited to performing simple in-mine experiments to test the validity of the theoretically predicted behavior at X-band frequencies.

TABLE VI

VARIATION OF THEORETICAL ATTENUATION RATES WITH FREQUENCY
FOR THE $E_{h,1,1}$ MODE IN A COAL MINE TUNNEL
FOR d_1 = 14 FT., d_2 = 7 FT., F = 1.0
K = 10, h = 4 IN., θ_o = 1°

Frequency MHz	Refraction α_{ref} (dB/100')	Roughness α_{rough} (dB/100')	Tilt α_{tilt} (dB/100')	Total α_{total} (dB/100')
200	25.50	1.05	.35	26.89
500	3.72	.42	.79	4.93
1,000	.92	.21	1.27	2.40
1,500	.41	.14	1.50	2.05
2,000	.23	.11	1.60	1.94
3,000	.10	.07	1.62	1.79
4,000	.06	.05	1.55	1.66
5,000	.04	.04	1.46	1.54
7,000	.02	.03	1.29	1.34
10,000	.01	.02	1.09	1.12

V. PROPAGATION AROUND A CORNER AND THROUGH A PILLAR

A. RAY PATH REFRACTION AND REFLECTION

Figure 12 shows what happens to a pair of parallel rays A and B, belonging to a low-order mode in a North-South tunnel, when they encounter two pillars. Ray A misses the first pillar and enters an East-West intersecting tunnel where it zig-zags between the two pillars at steep angles, corrsponding, on the wave picture, to a superposition of high order modes of the East-West tunnel. These modes attenuate rapidly by refraction, roughness, and tilt losses.

Ray B strikes the West wall of the first pillar where it is partly reflected and partly refracted into the pillar. The reflected ray remains in the original low-order mode since the grazing angle ϕ is unchanged after reflection. Note that the grazing angle has been exaggerated in Figure 12 to better illustrate the principles involved. The refracted ray is strongly bent, as shown, and proceeds in the limestone pillar at an angle with respect to the normal to the N-S wall that is slightly less than the critical angle C, which for K = 5 is 26.6°. The ray then strikes the E-W wall of the pillar at 63.4° with respect to its normal, which is well beyond the critical angle of 26.6° for the E-W wall. Total internal reflection therefore occurs, and no refracted ray enters the E-W cross tunnel. The ray next strikes a N-S wall at slightly less than the critical angle. Therefore refraction occurs and part of the ray enters the parallel N-S tunnel and travels southward at the correct mode angle in this tunnel. There is also an internally reflected ray which undergoes further reflections and refractions. It is to be noted, however, that refractions occur only at the N-S walls of the pillar. No rays enter the E-W tunnels from within the pillar.

The main effect of propagation through and around the pillars is, therefore, that the original low-order mode in a tunnel, produced by a distant transmitter, can be transferred to <u>parallel</u> tunnels, provided that attenuation in the limestone is not too large. No direct transfer of the low-order mode into 90° intersecting tunnels takes place.

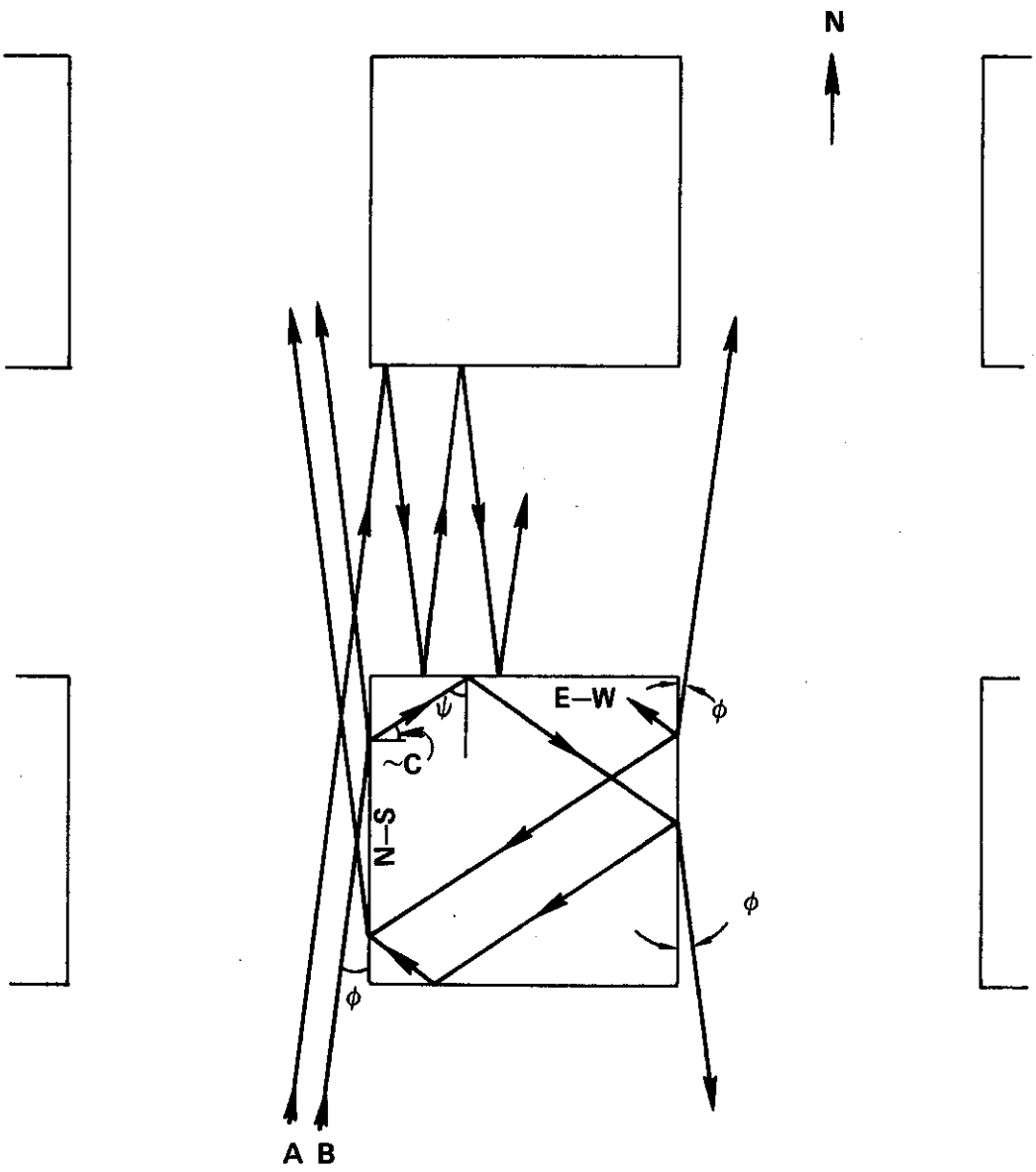

FIGURE 12 RAY DIAGRAM FOR PROPAGATION AROUND AND THROUGH A PILLAR

B. EVANESCENT WAVES

When total internal reflection occurs as shown in Figure 12, an evanescent wave exists in the cross tunnel just outside the E-W wall of the pillar. The electric field of this wave falls off with distance x from the wall according to the relation

$$E = E_o e^{-\alpha x} \quad , \tag{47}$$

where

$$\alpha = \frac{2\pi}{\lambda}\sqrt{(K-1) - K\cos^2\psi} \quad . \tag{48}$$

Here λ is the free-space wavelength, K is the dielectric constant of the limestone, and ψ is the internal angle of incidence at the wall. For the case illustrated in Figure 12, $\psi \approx 90° - C$. Therefore,

$$\cos\psi \stackrel{\sim}{=} \sin C = \frac{1}{\sqrt{K}} \tag{49}$$

and (47) becomes

$$\alpha = \frac{2\pi}{\lambda}\sqrt{K - 2} \quad . \tag{50}$$

Table VII shows values of α for K = 5, at the wavelengths of interest.

TABLE VII

EVANESCENT WAVE DECAY RATE

f (MHz)	λ (ft.)	α (Neper/ft.)	α (dB/ft.)
450	2.19	4.98	43.3
850	1.16	9.40	81.6

It is seen that the evanescent wave is of negligible amplitude at a distance of 1 foot from the wall. However, this conclusion is strictly valid only in the case of a perfectly smooth wall. If the wall is rough, the evanescent wave undergoes diffuse scattering to an extent

that depends on the magnitude of the ratio h/λ of the rms roughness to the wavelength. However, since the diffuse radiation is almost isotropic, it does not significantly excite the desirable low-order modes of the E-W tunnel which are concentrated at small grazing angles.

C. ATTENUATION RATE IN LIMESTONE

The efficiency of transfer of a low-order mode from one tunnel to a parallel tunnel by transmission through pillars, as illustrated in Figure 12, depends on the electrical conductivity of the limestone. The attenuation and phase constants, α_L and β_L, for propagation in the limestone are given by the real and imaginary parts of the equation

$$\alpha_L + i\beta_L = (-4\pi^2 f^2 \mu_o \varepsilon_o K + i2\pi f \mu_o \sigma)^{1/2}, \tag{51}$$

where μ_o, ε_o are the magnetic and electric permittivities of free space, K is the dielectric constant of limestone, and σ is the conductivity of limestone.

Table VIII shows how α_L depends on frequency and conductivity.

TABLE VIII

ATTENUATION RATE IN LIMESTONE

f (MHz)	σ (Mho/m)	α_L (dB/ft.)
450	10^{-1}	20.89
	10^{-2}	2.229
	10^{-3}	0.2231
850	10^{-1}	21.843
	10^{-2}	2.231
	10^{-3}	0.2231

It is seen that α_L depends very slightly on frequency, but varies almost linearly with conductivity. Since the pillar cross-sectional dimensions are 35 ft. x 35 ft., the shortest path of a ray from the left-hand to the right-hand tunnel is about 42 ft. The minimum

attenuations are therefore 880 dB, 94 dB, and 9 dB, respectively, for conductivities of 10^{-1}, 10^{-2}, and 10^{-3} Mho/m. If values of limestone conductivity[6] are more likely to be in the vicinity of 10^{-2} than 10^{-3} Mho/m, it appears that mode transfer to a parallel tunnel will not be significant in most cases. However, in those cases where the conductivity is close to 10^{-3} Mho/m, a usable amount of coupling to the parallel tunnel will occur. Furthermore, qualitative data taken by Chufo and Isberg[1] in parallel tunnels at the Black River limestone mine appear to support the existence of this behavior at this mine.

VI. REFERENCES

1. R. L. Chufo and R. A. Isberg, "Passive Reflectors as a Means for Extending UHF Signals Down Intersecting Crosscuts in Mines or Large Corridors," Conference Record, Twenty Eighth IEEE Vehicular Technology Conference, Denver, Colorado, IEEE Cat. No. 78CH1297-1VT, pp 267-272, March 22-24, 1978.

2. R. A. Isberg, "UHF Radio System Tests in Black River Mine," Collection of Informal Field Test Reports to U. S. Bureau of Mines, Nov. 14-18, 1977.

3. R. Chufo, Graphs of Data Taken at Black River Limestone Mine, Informal Communication, 1978.

4. A. G. Emslie, R. L. Lagace, and P. F. Strong, "Theory of the Propagation of UHF Radio Waves in Coal Mine Tunnels," IEEE Trans. on Antennas and Propagation, Vol. AP-23, No. 2, pp 192-205, March 1975.

5. J. V. Nickel and L. Burkett, "800 MHz Radio Communications for Underground Mining," Proceedings of the Fourth WVU Conference on Coal Mine Electrotechnology, pp 26-1 to 11, August 2-4, 1978.

6. E. I. Parkomenko, "Average Electrical Properties of Large Masses of Rock," Figure 8, p. 294 in Supplementary Guide to the Literature on Electrical Properties of Rocks and Minerals by G. V. Keller, Electrical Properties of Rocks, Edited by G. V. Keller, 314 pp, Plenum Press, New York, 1967.

CAMBRIDGE,
MASSACHUSETTS

SAN FRANCISCO
WASHINGTON
ATHENS
BRUSSELS
LONDON
PARIS
RIO DE JANEIRO
TORONTO
WIESBADEN